Large Binocular Telescope image restoration using simulated adaptively corrected point-spread functions

S. Correia[a], M. Carbillet[a], A. Richichi[a,d], M. Bertero[b] and P. Boccacci[c],

[a]Osservatorio Astrofisico di Arcetri, Largo E. Fermi 5, I-50125 Firenze, Italy

[b]INFM and Department of Computer and Information Sciences,
University of Genova, Via Dodecaneso 35, I-16146 Genova, Italy

[c]INFM and Department of Physics, University of Genova,
Via Dodecaneso 33, I-16146 Genova, Italy

[d] European Southern Observatory,
Karl-Schwarzschildstr. 2, D-85748 Garching b.M., Germany

ABSTRACT

In this paper we present simulations of Large Binocular Telescope (LBT) image reconstruction carried out on different types of scientific objects. The set of Adaptive Optics-corrected point-spread functions (AO-corrected PSFs) used was generated by means of the Code for Adaptive Optics Systems (CAOS 2.0). For clarity only one restoration method was applied to the simulated data, namely the extension of the Lucy-Richardson (LR) algorithm, also called ML-EM (Maximum Likelihood - Expectation Maximization). When possible we evaluated the quality of the restorations obtained both by astrometric and photometric analysis. By comparison with results obtained using analytical PSFs, we point out the effect induced by the AO correction on the precision of the retrieved astrometric and photometric parameters or on the morphology of the reconstructed object.

Keywords: image reconstruction, interferometry, adaptive optics, Large Binocular Telescope

1. INTRODUCTION

The Large Binocular Telescope (LBT) will consist of two 8.4 m mirrors placed 14.4 m apart on a common alt-azimuth mount.[1] Its special features, with respect to other interferometers, are the capacity to provide a large field of view and to allow a complete *uv* coverage. Additionally the foreseen high-level Adaptive Optics (AO) system, including the adaptive secondary mirror[2] and further new techniques, like multi-conjugate AO[3] and laser-star tomography, is intended to achieve an high quality correction on a large part of the field.

However, in order to be able to produce high resolution imaging from LBT data, one has to combine different informations on the object coming from different orientations of the baseline. In addition, imaging techniques must be able to correct alterations coming from the transfer function of the telescope. For these reasons, multiple images deconvolution techniques are used to achieve this goal. Given the ill-posedness of the deconvolution problem,[4] the scientific exploitation of the reduced data has to be carried out carefully. Furthermore, one has to take into account that the knowledge of the interferometric point-spread function (PSF) used in the deconvolution process is limited. Such a limiting factor resides in the difference of AO compensation achieved for the point-like object of the field used as PSF with respect to that obtained on the scientific object. Some imaging tests were performed in order to estimate the precision and accuracy attainable under such a condition.[5] In this first test we dealt with real LBT-like data coming from a scaled experiment performed at the 1.5 m infrared TIRGO telescope.

In the present paper we present numerical simulations of image restoration performed on different kinds of scientific objects using simulated LBT AO-compensated PSFs. These sets of PSFs were computed by means of the Code for Adaptive Optics Systems (CAOS 2.0).[6,7] We focus on the comparison between restorations obtained using ideal PSFs and those using AO-corrected ones. In particular we compare the astrometric and photometric precision attained in these two cases.

E-mail addresses: Serge Correia: correia@arcetri.astro.it, Marcel Carbillet: marcel@arcetri.astro.it, Andrea Richichi: richichi@arcetri.astro.it, arichich@eso.org, Mario Bertero: bertero@disi.unige.it, Patrizia Boccacci: boccacci@fisica.unige.it

In Sect. 2 we briefly summarize the parameters used for the generation of AO-corrected PSFs, the pre-processing performed on these PSFs before deconvolution and we recall the restoration method. In Sect. 3 the results concerning the numerical simulation of image restoration are presented.

2. SIMULATED AO-CORRECTED PSFS AND IMAGE RESTORATION METHOD

Two sets of LBT interferometric AO-corrected PSFs have been generated by means of the Code for Adaptive Optics Systems (CAOS 2.0). A complete description of the simulation and details about the results can be found in Carbillet et al.[7] Here we only summarize some parameters of particular interest and describe the pre-processing performed before application of the deconvolution process.

A first set of PSFs corresponds to the natural guide star used for wavefront sensing measurements and a second one corresponds to the scientific object. In the following, the first set of PSFs will be used as reference-PSFs in the process of image reconstruction. The second one will be used as object-PSFs to form the interferograms by convolution with the object. Each set contains PSFs computed for three orientations of the baseline, that is at parallactic angle $0°, 60°$ and $120°$. These data have been simulated in R-band, with an angular separation between the guide star and the scientific object of $0\farcs3$. All PSFs here were assumed as monochromatic PSFs i.e. bandwidth was not taken into account. We assumed a $R = 9.25$ guide star magnitude and an integration time of 2.5 s. Time averaging smearing, that is the rotation of the projected baseline on the object during exposure, was considered negligeable for such an integration time. The spatial sampling adopted was 3 pixels/FWHM of the fringes, where the FWHM of the fringes is equal to λ/L, with L the total baseline length, here $L = 22.65$ m, and λ the filter central wavelength. For this observation band the value of the pixel size came 2.13 mas. The main parameters chosen for the turbulent atmosphere were: a Fried parameter r_0 of ~ 25 cm at 700 nm, a wavefront outer scale L_0 of 60 m, two equally turbulent layers at height 0 m and 10000 m respectively, with perpendicular winds with a speed of $5\,m.s^{-1}$. For each reference-PSF and interferogram, we assumed 30 % efficiency (mirror + optics + detector), a read-out noise of $2\,e-$ RMS and a sky background brightness of 20.0 mag/arcsec^2. The level of AO-correction obtained with this simulation is characterized by an averaged Strehl ratio (SR) of 0.16 and 0.14 for respectively the reference-PSFs and the object-PSFs sets. Pre-processing consisted in a re-centering of each PSF frame on the pixel closest to the centroid location. Since the relatively short integration time considered here, we did not attempt any sky background subtraction.

In this work we made use of a modification of the Lucy-Richardson algorithm (LR) which applies to the restoration of multiple images of the same object. The origin of this algorithm is indeed the so-called Maximum Likelihood - Expectation Maximization (ML-EM). Details of this algorithm and extensions to other computed-tomographic methods applied to the case of LBT image restoration, including numerical simulations as well, can be found in Bertero et al.[8,9]

3. SIMULATION RESULTS

3.1. Binary object

We assumed a binary object of separation 12 mas, e.g. a binary star of our galaxy at a distance of 1 kpc and with an apparent separation of 12 AU. This angular separation corresponds to about 1.5 times the resolution limit as defined by the Rayleigh criterion, that is 1.22 λ/L. In the R-band considered here, this resolution limit is 7.8 mas. The position angle was arbitrarily set to 36 degrees. The magnitude of the primary was $R = 20$ and the magnitude difference $\Delta R = 2$. The process of interferogram computation consisted in a numerical convolution of the object with the object-PSF of each parallactic angle, both up-sampled four times with respect to the detector grid. Each frame has been rebinned afterwards in the detector grid and corrupted by noise. With the parameters adopted here, the peak SNR and the number of e-photons of each simulated interferogram was in average 14 and 1.4 10^4 respectively.

The detection of each star on the reconstruction frame has been achieved by an ad hoc routine, which detects on the frame the peak location over a threshold value and masks the pixels around before continuing. Parameters of such a routine were a detection radius of about 6 mas, i.e. approximately twice the fringes FWHM, and a threshold detection of the star from the background set to 50 in background units. Centroid calculations were carried out with 5×5 pixels box size centered on each detected star peak pixel. Aperture photometry was computed with aperture diameter of 3, 4 and 5 pixels centered on the detected centroid location. In our case 5 pixels aperture diameter is the maximum in order to not overlap the apertures. In addition we monitored the convergence of both these astrometric

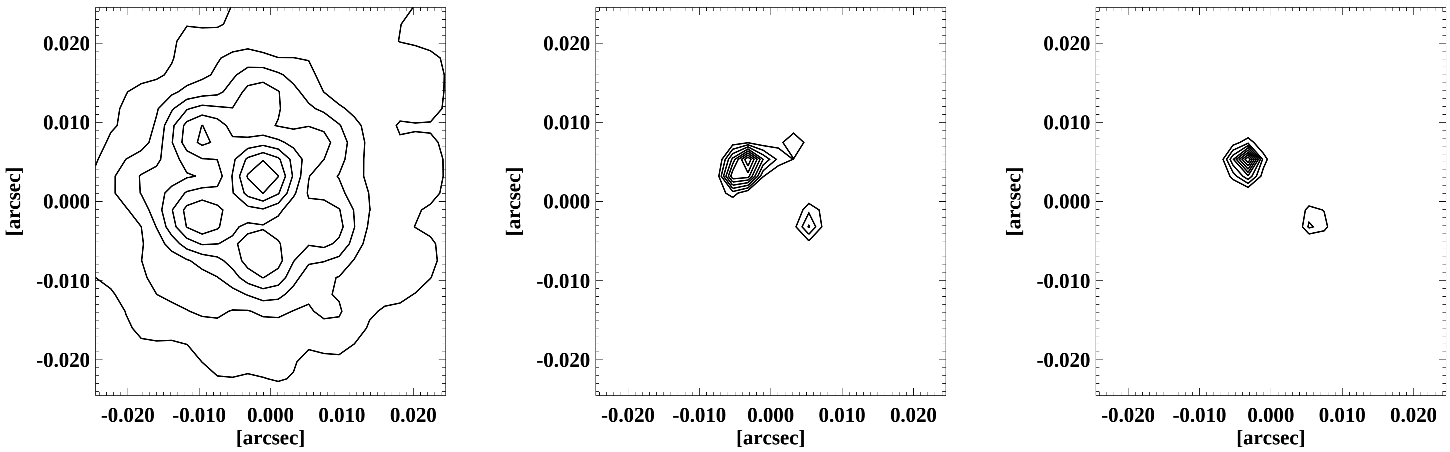

Figure 1. From left to right: Incoherent sum of the the binary object interferograms with adaptively corrected PSFs, restored frame with adaptively corrected PSFs and restoration obtained with ideal PSFs. Frames are displayed using a power law scale of factor 0.5. Contour levels are from 20% to 100% of the maximum, in steps of 10%.

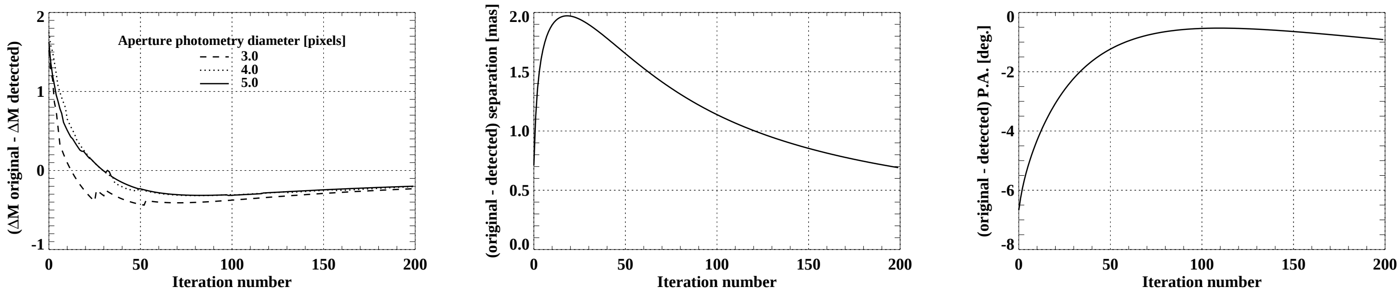

Figure 2. Convergence plots of the photometric and astrometric parameters in the AO-corrected case. Original minus detected values as a function of the number of iteration for, from left to right, the difference of magnitude ΔM, the angular separation and the position angle PA. The pixel size is 2.13 mas.

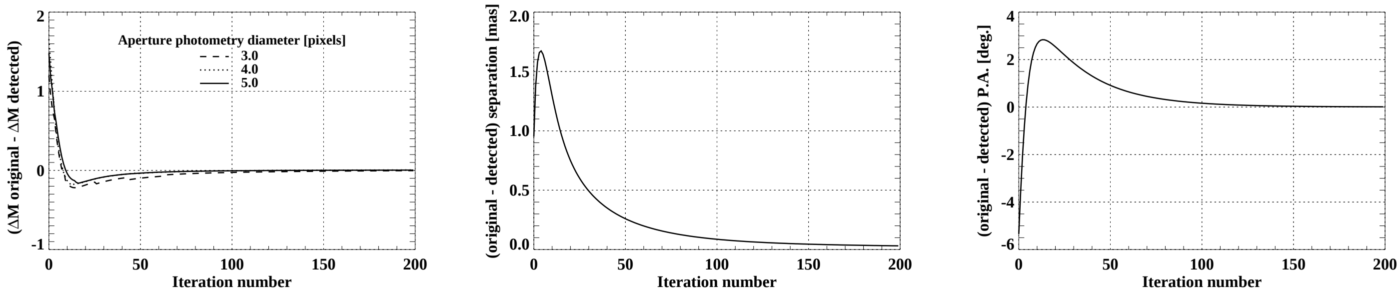

Figure 3. Same convergence plots as in Fig. 2 but for the ideal case.

Table 1. Original minus detected values of the binary parameters in the AO-corrected PSFs case compared to the analytical PSFs case.

	AO-corrected PSFs	analytical PSFs
ΔR	- 0.20	$3.8\ .10^{-3}$
$\Delta separation$ [mas]	0.69	$3.1\ .10^{-2}$
$\Delta P.A.$ [degree]	- 0.92	$1.1\ .10^{-2}$

and photometric parameters with iteration number. This was done using the location of each star in each iterated frame.

In the following we compare results obtained with AO-corrected PSFs with those obtained with ideal PSFs. Figure 1 shows the incoherent sum of the binary object interferograms with AO-corrected PSFs and the reconstructed object for 200 iterations of the LR algorithm with AO-corrected PSFs compared to the result obtained with ideal PSFs.

Figure 2 and 3 show the convergence plots for respectively the AO-corrected case and the ideal case. A general remark concerning these plots is that, in spite of the lack of a real stopping rule for the LR algorithm, the convergence behaviour presented by these plots gives enough confidence on the reliability of the retrieved parameters. Each figure presents the original minus detected values of the binary parameters in function of iteration number. One can note that the AO-corrected case presents a slower convergence with respect to the ideal case. Excepted for the P.A., 200 iterations does not seem to permit a complete convergence to occur.

We report in Table 1 the relative values of the binary parameters corresponding to the last iteration for the two cases considered here. One can define a so-called degradation factor as the ratio of the absolute value of these two quantities for each parameter. This factor takes globally values of a few ten to almost an hundred. In case of AO correction, the precision attained on the difference of magnitude and on the angular separation are respectively of 10% and 5.8%. This represents a good result if one take into account the average SNR of the frames and the original separation of the binary. One can also note that 0.69 mas and 0.92 degrees represents respectively about one third of the pixel size and one tenth of the angular size of a pixel for this binary separation. Furthermore the level of AO correction considered here is relatively low (SR $\sim$ 0.16), and a gain of precision is therefore possible yet. A difficult task of deconvolution is to estimate the error on the values measured on deconvolved frames. A possible way in a future work could be to consider different sets of AO-corrected PSFs, at different correction levels, in order to deduce a statistic on the retrieved parameters.

3.2. Star cluster

The model we used in the following simulations is a synthetic star cluster. A list of star coordinates and magnitudes was generated by the IRAF task Starlist, for a sample of 100 stars. We selected an Hubble spatial density function defined by the relative spatial density function P as :

$$P = \frac{1}{(1+\frac{R}{R_0})^2} + C \qquad (1)$$

where R is the radial distance, R_0 the core radius of the distribution and C the relative background density. In our simulation, considering a field of view of $0\farcs27$ (128×128 pixel array), we set $R_0 = 64\ mas$ (30 pixels) and $C = 0$. We chose the Bahcall and Soneira luminosity function and generated relative magnitudes values between -7 and 0. This luminosity function is a best fit of observed main sequence stars in several nearby globular cluster. The zero-point of the magnitude was set in order to obtain a star cluster with star magnitudes ranging from 8 to 14 in R-band. An up-sampling similar to the binary object case was performed in order to conserve the information of the sub-pixel location of the stars in the simulated observations.

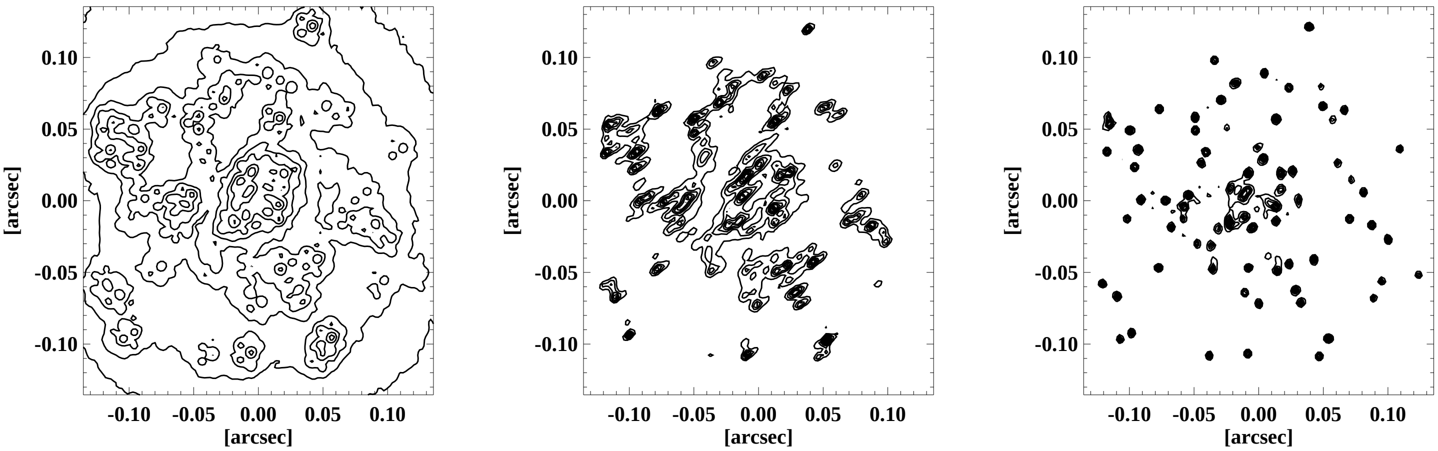

Figure 4. From left to right : Incoherent sum of the the star cluster interferograms with adaptively corrected PSFs, restored frame with AO-corrected PSFs and restoration obtained with ideal PSFs. Frames are displayed using a power law scale of factor 0.5. Contour levels are from 10% to 100% of the maximum, in steps of 10%.

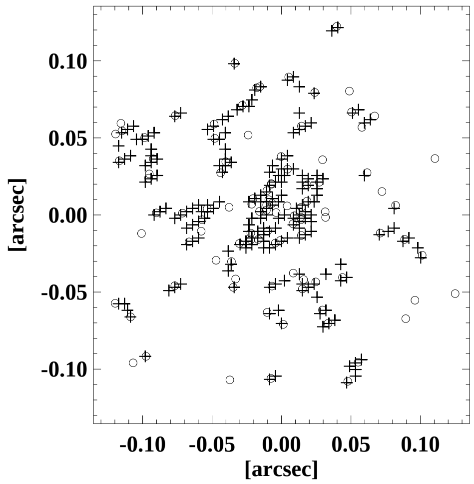

Figure 5. Detected star location of the restored frame in the AO-corrected case (crosses) display on the original star locations (circles). We show here the first 200 stars detected by the same routine used in Sect. 3.1 with a detection radius equal to the resolution limit.

Figure 4 shows the incoherent sum of the star cluster interferograms with AO-corrected PSFs and the reconstructed object for 200 iterations of the LR algorithm with AO-corrected PSFs, compared to the result obtained with ideal PSFs. One can note that the restoration in the AO-corrected case shows an overall elongated shape of the stars. This feature is also visible on the binary object restoration with AO-corrected PSFs and is probably due to the residual energy presents in the halo of these PSFs. However in this crowded star field the effect of such a phenomenon appears with more acuteness. As a consequence, the detection of the star location on the restored frames is strongly biased (Fig. 5). One can note that several non-existing stars are found and that some real stars are not detected.

3.3. Young binary with circumstellar matter

We used as object an high angular resolution image of the T Tauri star GG Tau obtained with AO compensation and LR deconvolution techniques.[10] This image presents a close binary pair surrounded by a bright elliptical circumbinary ring which represents the inner limit of a larger circumstellar disk containing bright spoke features.

For our simulation we considered the J-band image, recovering its original dynamic range. Because we assumed observations carried out in R-band, we had to rescale the flux coming from the light scattered by the circumstellar matter with respect to the flux coming from the close binary. This was done by considering an extinction coefficient ratio $A_R/A_J = 2.65$ corresponding to typical interstellar dust.[11] The flux coming from outside the binary was

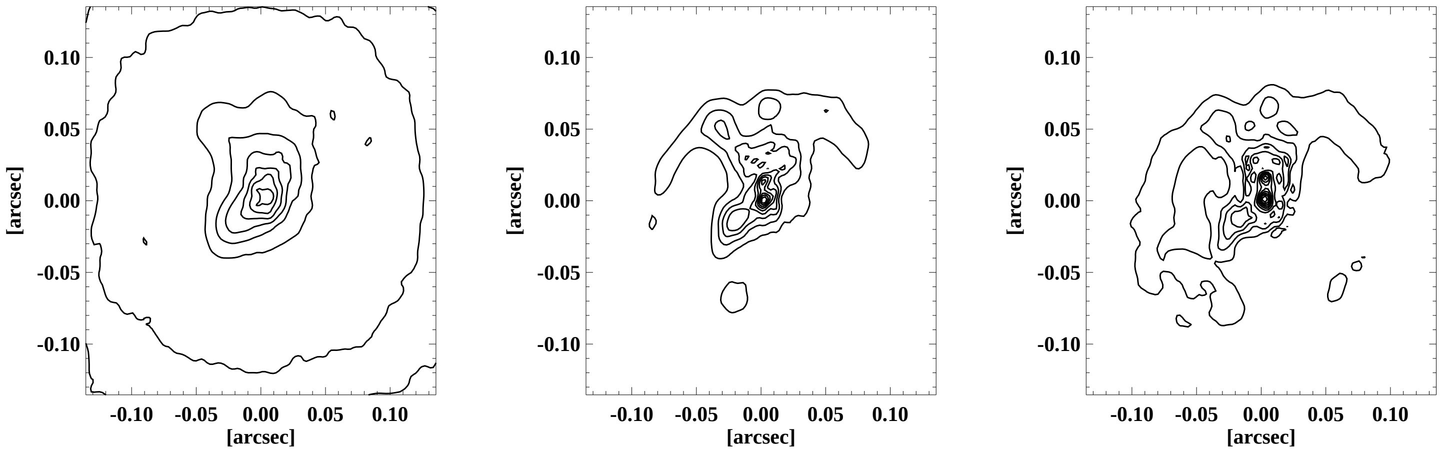

Figure 6. From left to right : Incoherent sum of the young binary star environment interferograms with adaptively corrected PSFs, restored frame with AO-corrected PSFs and restoration obtained with ideal PSFs. Frames are displayed using a power law scale of factor 0.3. Contour levels are from 10% to 100% of the maximum, in steps of 10%.

then scaled and the flux coming from the binary used as a calibration source. Therefore assuming $R = 11.76$[12] for the binary leads to $R = 10.96$ with the surrounding emission included. The object was scaled to fit in our 128×128 pixel array with the resulted $0\farcs27$ field of view. With an initial distance of 140 pc, the scaled object is about 17 times farther at 2.4 kpc. The scaled close pair presents an angular separation of about 14.9 mas with a total magnitude $R = 17.9$. We did not attempt to scale the difference of magnitude from J-band to R-band as a consequence of the different spectral types of the two components. Therefore the difference of magnitude was kept around 0.88. The binary parameters have been calibrated in the object frame with the same routine used to achieve the measurements into the restored frames. Calibrated values were then $\Delta R = 1.04$ for the difference of magnitude, an angular separation of 14.8 mas and a position angle of 273.5 degrees.

Figure 6 shows the incoherent sum of the object interferograms with AO-corrected PSFs and the reconstructed object for 200 iterations of the LR algorithm with AO-corrected PSFs, compared to the result obtained with ideal PSFs.

Concerning the object morphology one can notice that in case of AO correction the circumbinary ring appears substantially smooth and presents the same residual elongated distortion encountered before, whereas with ideal PSFs the ring comes sharper but also with some amount of azimuthal distortions. The left frame of Fig. 7 shows the deconvolution of the object blurred by the analytical PSF corresponding to a 22.65 m diameter telescope and can be considered as the reference object image. Without taking into account the first contour, that is 5.10^{-4} of the maximum, the shape and brightness of the circumstellar environment are, in both interferometric restored frames, well in agreement with this reference, and do not present any significant difference. In particular the position and brightness of the upper left and down left bright knots are well retrieved in both cases. Actually, these features can already be seen on the restored frames corresponding to the single apertures (right and middle frames of Fig. 7). Obviously the reason is that these features have a relatively large extension and hence do not require an high resolution to be imaged.

Different is the case of the central object, the close pair, that can be resolved only with a higher resolution. Indeed, as we expected, it is not resolved on the single aperture deconvolved frames but it is on the interferometric reconstructed frames. Figure 8 and Fig. 9 show the convergence plots of the binary parameters relative to the calibrated values for respectively the AO-corrected case and the ideal case. We also report these values for the last iteration in Table 2. We note a relatively minor discrepancy between the two cases that in Sect. 3.1. The degradation factor is typically a few units. Whereas the close pair is brighter and more separated than the binary object considered in Sect. 3.1, the precision obtained in both AO-corrected and ideal case is lower here. This is especially true for the astrometric parameters. It can be seen as a consequence of the presence of distortions coming from the surrounding

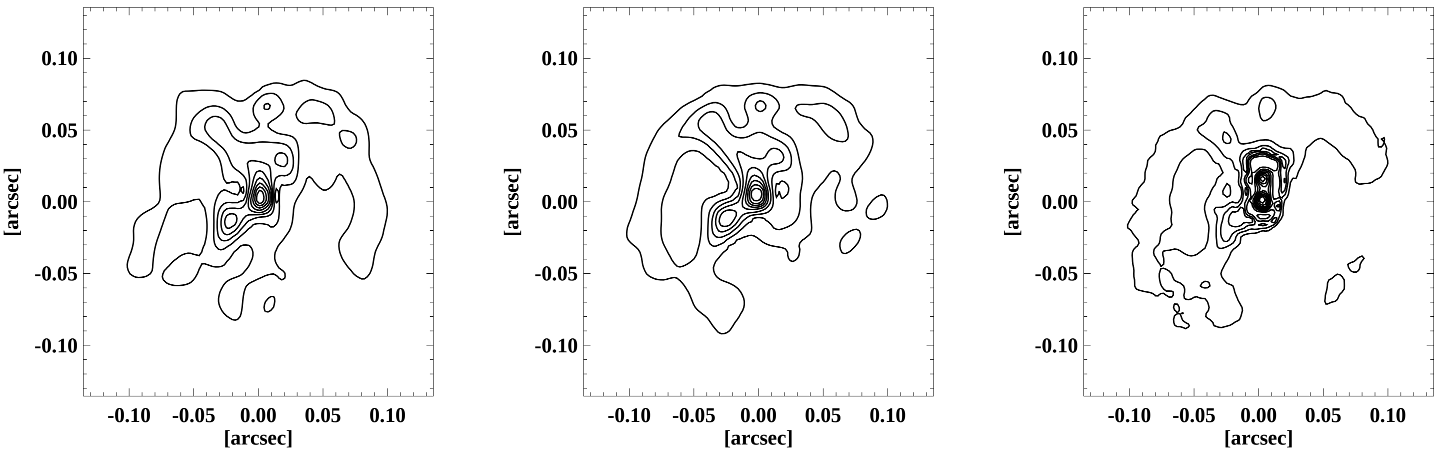

Figure 7. Deconvolved frames of the young binary star environment originally blurred by the AO-corrected single (8.25 m) PSF corresponding to the east pupil (left) and west pupil (middle), and originally blurred by the ideal PSF corresponding to a 22.65 m diameter telescope (right). We considered 200 iterations of the LR algorithm and 3 times more photons for the 22.65 m case respect to both 8.25 m cases. This was done in order to allow a direct comparison with the interferometric reconstruction. Frames corresponding to the 8.25 m deconvolution have been rebinned into the usual frame size for comparison. Note that the difference between the two single pupil deconvolution results came essentially from the difference between the two single pupil PSFs. This is a consequence of the short integration time considered here. Frames are displayed using a power law scale of factor 0.3. Contour levels are from 10% to 100% of the maximum, in steps of 10%.

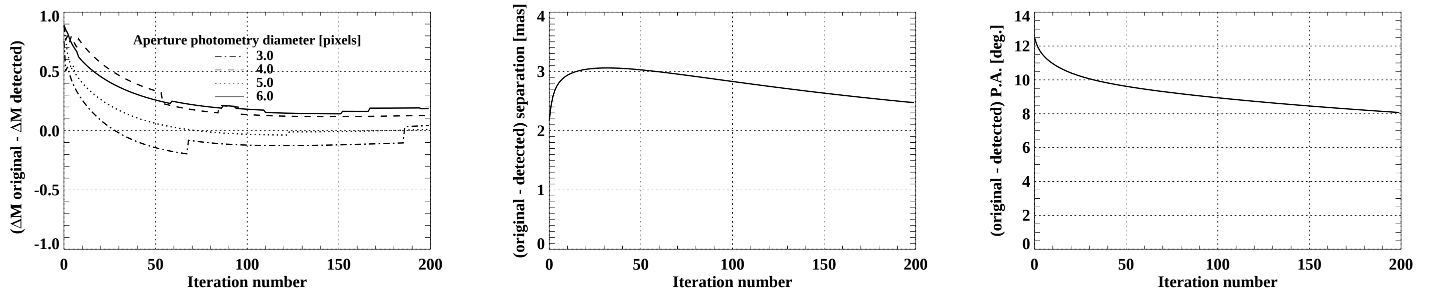

Figure 8. Convergence plots of the photometric and astrometric parameters in the AO-corrected case. Original minus detected values as a function of the number of iteration for, from left to right, the difference of magnitude ΔM, the angular separation and the position angle PA. The pixel size is 2.13 mas

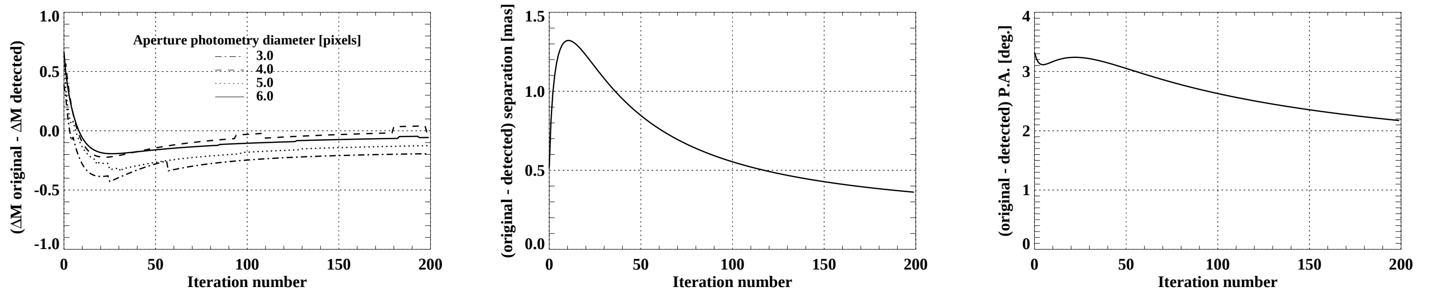

Figure 9. Same convergence plots as in Fig. 8 but for the ideal case.

Table 2. Original minus detected values of the young close pair parameters in the AO-corrected PSFs case compared to the analytical PSFs case.

	AO-corrected PSFs	analytical PSFs
ΔR	0.19	- 5.7 .10^{-2}
$\Delta separation$ [mas]	2.45	0.36
$\Delta P.A.$ [degree]	8.07	2.17

environment, particularly from the bright circumbinary ring.

4. CONCLUSIONS

Simulations of LBT image restorations using simulated adaptively corrected PSFs have been presented. These have been performed on some different scientific objects of interest. We have shown the effect on the results of the reconstruction that one can expect in case of AO correction with respect to the ideal case in which the turbulent atmosphere degradation is not taken into account. This comparison has been done both qualitatively, based on the morphology, and quantitatively, based on the precision of astrometric and photometric parameters. In the case of the binary object considered here we obtained a precision on the difference of magnitude of 0.2 corresponding to 10% of the original difference of magnitude. The precision on the separation and on the position angle is respectively of 0.69 mas (i.e. $\sim 1/3$ of the pixel size and 5.8% of the original value) and of 0.92 degrees (i.e. $\sim 1/10$ of the angular size of a pixel seen at this separation). The star cluster reconstruction presents a significant amount of PSFs residuals that prevents from the detection of a consequent number of stars and, in addition, leads to the detection of many non-existing stars. The young binary environment was found also to be affected by the same PSFs residuals, in the morphology as well as in the precision obtained on the parameters of the close pair. But for this last one, the presence of surrounding light emission regions constitutes also a significant, and probably the most important, factor of degradation.

ACKNOWLEDGMENTS

The authors whish to thank Bruno Femenía, Armando Riccardi, Guido Brusa and Simone Esposito for useful suggestions. Marcel Carbillet is supported by the TMR program funded by the European Union (contract nr. ERBFM-RXCT96 - 0094). This work was partially supported by CNAA (Comitato Nazionale per l'Astronomia e l'Astrofisica) under the contract nr. 16/97.

REFERENCES

1. J. R. P. Angel, J. M. Hill, P. A. Strittmatter, P. Salinari, and G. Weigelt, "Interferometry with the Large Binocular Telescope," in *Astronomical Interferometry*, R. D. Reasenberg, ed., *Proc. SPIE* **3352**, pp. 881–902, 1998.
2. C. Del Vecchio and D. Gallieni, "Numerical simulations of the LBT adaptive secondary mirror," in *Adaptive Optical Systems Technology*, P. L. Wizinowich, ed., *Proc. SPIE* **4007**, (Muenchen, Germany), 2000. Proceedings of this conference.
3. J. M. Beckers, "Increasing the size of the anisoplanatic patch with multiconjugate adaptive optics," in *Very Large Telescopes and Their Instrumentation*, M. H. Ulrich, ed., *Proc. ESO conference* **March 1988**, pp. 693–703, 1988.
4. M. Bertero and P. Boccacci, *Introduction to inverse problems in imaging*, Institute of Physics Publishing, Bristol, 1998.
5. S. Correia and A. Richichi, "Interferometric imaging tests for the Large Binocular Telescope," *Astron. Astrophys. Suppl. Ser.* **141**, pp. 301–310, 2000.
6. M. Carbillet, B. Femenía, F. Delplancke, S. Esposito, L. Fini, A. Riccardi, E. Viard, N. Hubin, and F. Rigaut, "LA^{3}OS^2: a software package for laser guide star adaptive optics systems," in *Adaptive Optics Systems and Technology*, R. K. Tyson and R. Q. Fugate, eds., *Proc. SPIE* **3762**, pp. 378–389, 1999.

7. M. Carbillet, S. Correia, B. Femenía, and A. Riccardi, "Adaptive optics simulations for imaging with the Large Binocular Telescope Interferometer : first results," in *Adaptive optical system technology*, P. L. Wizinowich, ed., *Proc. SPIE* **4007**, (Muenchen, Germany), 2000. Proceedings of this conference.
8. M. Bertero, P. Boccacci, S. Correia, and A. Richichi, "Tomographic methods for the restoration of LBT images," in *Interferometry in optical Astronomy*, P. J. Lena and A. Quirrenbach, eds., *Proc. SPIE* **4006**, (Muenchen, Germany), 2000. Proceedings of this conference.
9. M. Bertero and P. Boccacci, "Applications of the OS-EM method to the restoration of LBT images," *Astron. Astrophys. Suppl. Ser.* , 2000. to appear.
10. C. Roddier, F. Roddier, M. J. Northcott, J. E. Graves, and K. Jim, "Adaptive optics imaging of GG Tauri : optical detection of the circumbinary ring," *The Astrophysical Journal* **463**, pp. 326–335, 1996.
11. G. H. Rieke and M. J. Lebofsky, "The interstellar extinction law from 1 to 13 microns," *The Astrophysical Journal* **288**, pp. 618–621, 1985.
12. A. M. Ghez, R. J. White, and M. Simon, "High spatial resolution imaging of pre-main-sequence binary stars : resolving the relationship between disks and close companions," *The Astrophysical Journal* **490**, pp. 353–367, 1997.